Research Article | Vol. 29, No. 15 / 19 July 2021 / Optics Express 23142
Optics EXPRESS

Capacity of underwater optical wireless communication systems over salinity-induced oceanic turbulence channels with ISI

RUBÉN BOLUDA-RUIZ,* PEDRO SALCEDO-SERRANO, BEATRIZ CASTILLO-VÁZQUEZ, ANTONIO GARCÍA-ZAMBRANA, AND JOSÉ MARÍA GARRIDO-BALSELLS

Department of Communications Engineering, Andalucía Tech., University of Málaga, Málaga E-29071, Spain
*rbr@ic.uma.es

Abstract: Point-to-point underwater optical wireless communication (UOWC) links are mainly impaired by scattering due to impurities and turbidity in the open water, resulting in a significant inter-symbol interference (ISI) that limits seriously both channel capacity and the maximum practical information rate. This paper conducts, for the first time, the channel capacity analysis of UOWC systems in the presence of ISI and salinity-induced oceanic turbulence when the undersea optical channel is accurately modeled by linear discrete-time filtering of the input symbols. In this way, novel upper and lower bounds on channel capacity and mutual information are developed for non-uniform on-off keying (OOK) modulation when different constraints are imposed on the channel input. The results show that the capacity-achieving distribution, which is computed through numerical optimization, is discrete and depends on the optical signal-to-noise-ratio (SNR). Moreover, a non-uniform input distribution significantly improves the channel capacity of such systems affected by ISI and oceanic turbulence, especially at low optical SNR. Monte Carlo techniques are employed to test the developed bounds for different undersea optical channels with one, two and three casual ISI coefficients.

1. Introduction

Point-to-point underwater optical wireless communication (UOWC) has become consolidated as a promising candidate to provide long-distance and high-speed links for a wide variety of scientific and industrial purposes related to ocean observation that is essential for the Green Deal, as well as for transmitting large amounts of data through seawater with high security [1,2]. However, the dispersive nature of the UOWC channel leads to an undesirable effect of inter-symbol interference (ISI) due to impurities in the seawater, not only limiting the achievable transmission rate severely, but also reducing link reliability [3]. To this impairment we may add the fact that small variations in salinity and temperature can lead to an optical signal fading called oceanic turbulence, degrading the overall performance of such systems [1,2]. Therefore, finding the capacity and the maximum practical information rate that can be used over the undersea optical channel with ISI in different practical scenarios such as clear ocean and coastal waters is a great challenge from an information-theoretical viewpoint.

The performance of UOWC systems has been extensively investigated for the past ten years mainly in terms of the bit error rate (BER) and outage probability by including different degrading factors such as absorption and scattering, temperature- and salinity-induced oceanic turbulence following different statistical distributions such as log-Normal, Weibull and exponential-generalized Gamma to name a few, as well as angular pointing errors due to water flows and random sea surface slopes [4–10] (and references therein). These reports demonstrated that an accurate channel model is crucial to permit a complete, realistic system design. Simultaneously,

#430200 https://doi.org/10.1364/OE.430200
Journal © 2021 Received 28 Apr 2021; revised 31 May 2021; accepted 1 Jun 2021; published 7 Jul 2021

Optics EXPRESS

numerous experiments have been conducted to measure the performance of UOWC systems under laboratory conditions such as in-pool testing that further prove their feasibility to provide long-distance and high-speed undersea links [11–13]. In [11], spread spectrum techniques are used to achieve a 42 m link when employing a laser diode (LD) in the blue-green band. A data rate of 5 Gbps was reported at a distance of 50 m using a discrete multi-tone transmission [12]. By employing on-off keying (OOK) modulation, a data rate of 2.7 Gbps was reported at a distance of 34.5 m [13]. Both BER and outage performance have been analyzed to some extent, however channel capacity analysis has not received enough attention yet and there is not much work done in this regard [14–19]. Moreover, these analysis are based on the Shannon's information theory and, hence, they are not simple to approach in practice. In [14], the average channel capacity for a buoy-based multiple-input/multiple-output UOWC system is analyzed in the presence of log-Normal oceanic turbulence. In [15], a pointing error model inherited from terrestrial free-space optical (FSO) communication systems is used to investigate the capacity over log-Normal oceanic turbulence channels. Similar capacity results are obtained in [16] under strong oceanic turbulence conditions. In [17,18], channel capacity is analyzed over oceanic turbulence channels by using the Málaga distribution. The impact of adaptive optics on channel capacity has been also studied under weak oceanic turbulence conditions [19]. As a general viewpoint, all these reports focus on examining the influence of oceanic turbulence on channel capacity, concluding that such an oceanic turbulence reduces considerably the capacity. These investigations into channel capacity, however, do not take into account the impact of ISI. In other words, the temporal dispersion produced by scattering is not taken into account when analyzing the channel capacity of UOWC systems. In contrast to terrestrial FSO systems, the dispersive nature of the undersea optical channel impacts drastically on the overall performance. As concluded in [20,21], UOWC links result in being noisy channels with finite memory that can be modeled by linear discrete-time filtering of the input symbols. Thus, analyzing how the effect of ISI degrades channel capacity of UOWC systems is certainly of real interest and needs to be quantified for communication purposes. Historically, the study of capacity of the discrete-time Gaussian channel in the presence of ISI has been addressed where both channel capacity and information rate have been estimated under different constraints imposed on the channel input [22–26].

In this paper, new upper and lower bounds on the capacity of undersea optical channels corrupted not only by white Gaussian noise, but also by scattering-induced ISI and salinity-induced oceanic turbulence are presented in the context of UOWC systems using non-uniform signalling. The capacity derivation, which is found by using the discrete-time Fourier transform (DFT) of the equivalent discrete-time impulse response of the system, is obtained by bounding the mutual information when non-negative and average optical power constraints are imposed on the channel input. Additionally, when a binary input constraint is imposed on the channel input, new upper and lower bounds on channel capacity and mutual information are also provided for different undersea optical channels with one, two and three casual ISI coefficients. Both channel capacity and mutual information are then computed for practical UOWC scenarios. The obtained results demonstrate that channel capacity is clearly affected not only by oceanic turbulence as concluded in the current literature, but also by scattering-induced ISI. Monte Carlo simulation results are further illustrated to test the derived bounds.

The balance of this paper is organized as follows. The system and channel models under study are described in Section 2 where the DFT of the equivalent discrete-time impulse response of the system is modeled analytically. In Section 3, the channel capacity analysis is performed where different constraints are imposed on the channel input. In Section 4, numerical results for channel capacity and mutual information (MI) are discussed under different severity of scattering and turbulence conditions. Finally, Section 5 concludes the paper.

Optics EXPRESS

2. System and channel models

Let us consider a single-input/single-output UOWC system using non-uniform OOK modulation which is based on intensity-modulation and direct-detection (IM/DD) due to its low cost and implementation simplicity [27,28]. Here, a green LD operating at 532 nm is used at the transmitter side, as well as a circular receiver aperture is used at the receiver side. A direct consequence of this modulation scheme is that the input signal is non-negative as it is proportional to the light intensity. Additionally, for safety and practical reasons, both the average optical power and the amplitude of the transmitted intensity are limited [29]. Thus, the input-output relation of the discrete-time model of a pulse amplitude modulation (PAM) IM/DD channel with ISI and oceanic turbulence, as shown in Fig. 1, can be expressed as

$$Y_k = (1/p)RP_t\sqrt{T_b}hX_k * c_k + Z_k, \tag{1}$$

where R is the photodetector responsivity in amps per watt and is considered to be unity without loss of generality, P_t is the average optical power, T_b is the bit period, h represents the oceanic path loss and fading due to oceanic turbulence, $X_k \in \{0, 1\}$ are independent identically distributed (i.i.d.) random variables following a Bernoulli distribution with parameter p that represent the bits to be transmitted, the symbol * denotes convolution, and c_k is a finite-length sequence of real coefficients that represents the equivalent discrete-time impulse response of the system that is derived as

$$c_k = g(t) * \mathbb{C}(t) * f(t)|_{t=kT_b}, \tag{2}$$

where $g(t)$ is the transmitter filter, $\mathbb{C}(t)$ is the fading-free channel impulse response with unity area [21], and $f(t)$ is the matched filter, i.e, $f(t) = g(-t)$. Non-return to zero (NRZ) OOK modulation is considered here, so that $g(t)$ is a rectangular pulse of duration T_b. Lastly, Z_k are i.i.d. Gaussian random variables with zero mean and variance $\sigma_n^2 = N_0/2$, i.e., $Z_k \sim N\left(0, \sigma_n^2\right)$ which are computed as $Z_k = z(t) * f(t)|_{t=kT_b}$. For convenience, the UOWC channel output samples are expressed as

$$Y_k = (1/p)P_t\sqrt{T_b}hc_0X_k + (1/p)P_t\sqrt{T_b}h\sum_{n=1}^{M} c_nX_{k-n} + Z_k, \tag{3}$$

where the summation term represents the ISI , M is the length of the channel impulse response tail, $c_k \neq 0$ for $k = \{0, 1, \ldots, M\}$, and $\sum c_k = 1$. In practice, a finite number of input symbols are affected by the ISI since h is assumed to be a slow fading [6]. Under this scenario, h is considered to be fixed during the transmission of all the bits $X_n \; \forall \; n \neq k$ producing ISI to X_k [4,5,9].

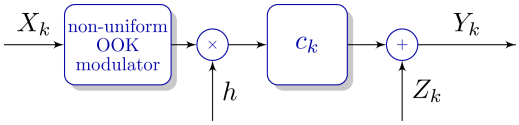

Fig. 1. Block diagram of the non-uniform baseband OOK system under study.

In order to derive new bounds on the capacity of UOWC channels with ISI in the next section, it is required to find the transfer function of the equivalent discrete-time impulse response c_k which is computed from the DFT as

$$C(\omega) = \sum_{n=0}^{M} c_n \exp\left(-jn\omega\right), \tag{4}$$

where $j = \sqrt{-1}$. Note that $C(\omega)$ is periodic in ω (normalized frequency) with period 2π. According to this study, c_k presents a decaying exponential, demonstrating that the energy of the

Optics EXPRESS

ISI coefficients decreases progressively. Hence, the frequency response of the UOWC system under study can be well approximated by $C(\omega) \simeq a\left(1 - be^{-j\omega}\right)^{-1}$ with $(a, b) \in \mathbb{R}^+$ and $0<b<1$, whose magnitude of the frequency response, $|C(\omega)|$, is readily obtained as

$$|C(\omega)| \simeq |\hat{C}(\omega)| = a\frac{\sqrt{1 + b^2 - 2b\cos\omega}}{1 + b^2 - 2b\cos\omega}, \tag{5}$$

where a can be computed as $a = c_0$, and b represents the impulse response tail as $b = \sum_{n=1}^{M} c_n$. As can be seen in greater detail in Appendix A, the approximation of the DFT of c_k is able to achieve a value of the coefficient of determination R-square (R^2) above 0.95 in almost all simulated cases. In Fig. 2, some examples of the magnitude of the frequency response of different UOWC channels are plotted when using a green LD with a transmit divergence angle of $\theta = 10$ mrad operating at $\lambda = 523$ nm with λ being the wavelength, as well as a photodetector diameter of $D = 20$ cm and a receiver field-of-view (FOV) value of 180°. Note that the results of the DFT of c_k obtained from Monte Carlo simulations are depicted with a solid line, whereas the results of the approximate DFT of c_k defined in Eq. (5) are depicted with a dashed line. The DFT for an ISI-less UOWC channel, i.e., $M = 0$ and $c_0 = 1$, is also displayed in cyan color as a reference. From this figure, remarkable differences can be observed when comparing clear ocean water with coastal water. For instance, in clear ocean water, the effect of scattering is not significant and, hence, $|C(\omega)|$ is practically flat $\forall\ |\omega| \leq \pi$, allowing a quasi ISI-free transmission through seawater at moderate distances. Besides, the Nyquist criterion for no ISI is satisfied in this scenario [30]. These results are further aligned with early reported works [20,21]. However, this conclusion cannot be drawn from coastal waters since scattering is much more severe due to a higher concentration of planktonic matter, among others, compared to clear ocean water [20]. Therefore, it may be anticipated that the ISI will present a greater impact on channel capacity for coastal water than for clear ocean water. These channels will be used to obtain upper and lower bounds on channel capacity of the UOWC system under study. It is also noteworthy to mention that the channels depicted in Fig. 2 are not unique and, hence, other UOWC channels with ISI may take place, depending on different aspects related to the communication system itself such as the characteristics of the transmitter and receiver, the symbol period, the link distance, as well as other major system parameters.

2.1. Statistical fading model

Oceanic path loss and salinity-induced oceanic turbulence are represented by $h = Lh_o$. The parameter L is computed from a modified version of the Beer Lambert's law to include scattering and geometric loss for a narrow LD with a Gaussian profile, as presented in [21, Eq. (11)], as

$$L \simeq \left(\frac{D/2}{d \cdot \theta}\right)^2 \times \exp(-F \cdot \alpha_T \cdot d), \tag{6}$$

where D is the photodetector diameter, θ is the transmit divergence angle, F is a correcting factor to include scattering [21], and d is the link distance. The extinction coefficient, α_T, is defined as the sum of absorption (α_1) and scattering (α_2) [3], whose values for a wavelength of 532 nm are summarized in Table 1.

Table 1. Extinction coefficient values for λ = 523 nm.

Water type	$\alpha_1[m^{-1}]$	$\alpha_2[m^{-1}]$	$\alpha_T[m^{-1}]$
Clear ocean water	0.114	0.037	0.151
Coastal water	0.179	0.219	0.398

Optics EXPRESS

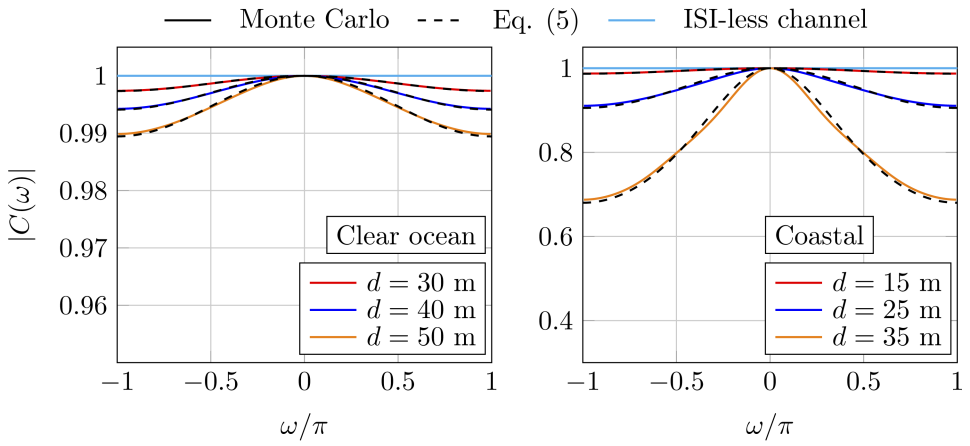

(a) R_b = 0.5 Gbps

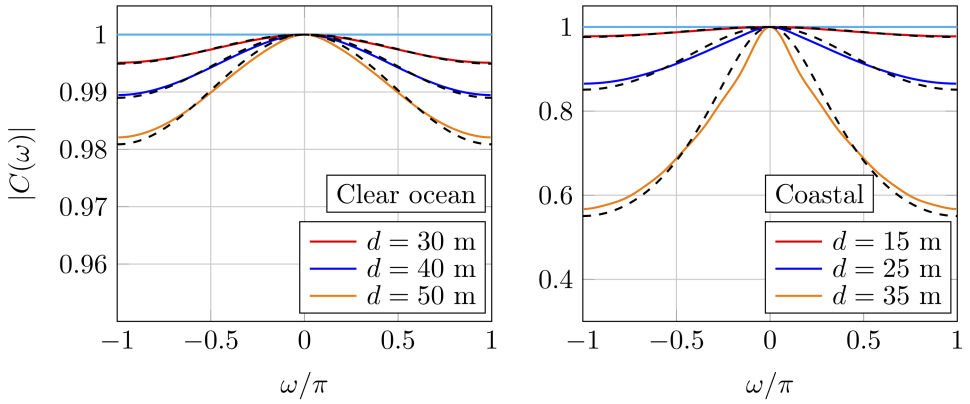

(b) R_b = 1 Gbps

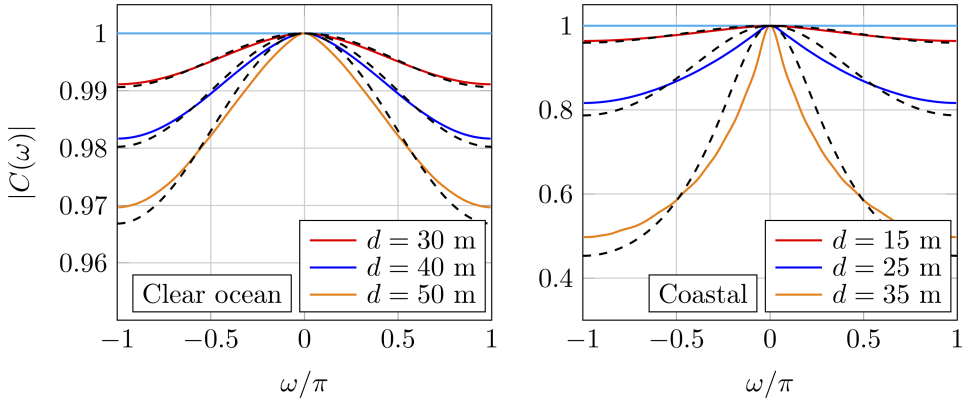

(c) R_b = 2 Gbps

Fig. 2. Examples of magnitudes of the frequency response, $|\hat{C}(\omega)|$, for $|\omega| \leq \pi$ of UOWC channels with ISI that model different severity of scattering conditions when a photodetector diameter of D = 20 cm and a FOV of 180° are used. These magnitude response results correspond to the UOWC system under study which employs NRZ OOK modulation for data rate values of $R_b = \{0.5, 1, 2\}$ Gbps and different link distances.

Optics EXPRESS

Oceanic turbulence, h_o, is accurately modeled according to the Weibull distribution [6,31], whose probability density function (PDF) with parameters β_1 and β_2 is given by

$$f_{h_o}(h) = \frac{\beta_1}{\beta_2}\left(\frac{h}{\beta_2}\right)^{\beta_1-1} \times e^{-\left(\frac{h}{\beta_2}\right)^{\beta_1}}, \quad h \geq 0. \tag{7}$$

The above PDF is currently being adopted to describe statistically oceanic turbulence that is present in the open waters and oceans with salinity gradient [6,7,21,31,32]. Some mathematical expressions were developed in [6] for β_1 and β_2, yielding

$$\beta_1 \simeq \left(\sigma_{h_o}^2\right)^{-6/11}, \tag{8a}$$

$$\beta_2 = 1/\Gamma\left(1 + 1/\beta_1\right), \tag{8b}$$

where $\sigma_{h_o}^2$ is the scintillation index of oceanic turbulence. Considering a plane-wave propagation as a limiting case of a collimated Gaussian beam propagation through seawater, $\sigma_{h_o}^2$ is defined, as in [33], as

$$\sigma_{h_o}^2 = 8\pi k^2 d \int_0^1 \int_0^\infty \kappa \Phi_n(\kappa)\left\{1 - \cos\left(\frac{d\kappa^2}{k}\xi\right)\right\} d\kappa d\xi, \tag{9}$$

where k is the wavenumber, and $\Phi_n(\kappa)$ is the power spectrum of oceanic turbulence fluctuations. Assuming isotropic and homogeneous waters with respect to salinity and temperature, $\Phi_n(\kappa)$ was derived in [34] as

$$\Phi_n(\kappa) = 0.388 \times 10^{-8} \epsilon^{-1/3} \kappa^{-11/3}\left[1 + 2.35(\kappa\eta)^{2/3}\right]\frac{\chi_T}{w^2}\left(w^2 e^{-A_T\delta} + e^{-A_S\delta} - 2we^{-A_{TS}\delta}\right), \tag{10}$$

where $\epsilon \in [10^{-8}, 10^{-2}]\ m^2/s^3$ represents the rate of dissipation of turbulent kinetic energy per unit mass of fluid, $\eta = 10^{-3}$ m is the Kolmogorov microscale that can take values varying from 6×10^{-5} m in strong turbulence conditions to 0.01 m in weak turbulence conditions, $\chi_T \in [10^{-10}, 10^{-4}]\ K^2/s$ is the rate of dissipation of mean-square temperature, $A_T = 1.863 \times 10^{-2}$, $A_S = 1.9 \times 10^{-4}$, $A_{TS} = 9.41 \times 10^{-3}$, $\delta = 8.248(\kappa\eta)^{4/3} + 12.978(\kappa\eta)^2$, and $w \in [-5, 0]$ represents the relative strength of temperature and salinity fluctuations [34–36].

3. Channel capacity analysis

In this section, upper and lower bounds on channel capacity of UOWC systems in the presence of ISI and salinity-induced oceanic turbulence are obtained when different constraints are imposed on the input channel. The basic for the discrete-time Gaussian channel with ISI developed in the previous section will be used to compute both channel capacity and mutual information for such communication systems.

3.1. Upper bound on channel capacity

In order to gain a better understanding of this analysis, let us start defining the capacity for a memoryless channel, i.e, when ISI does not take place or equivalently when $M = 0$ and $c_0 = 1$. According to [37, Chapter 10], the capacity in bits per channel use for a discrete-time memoryless Gaussian channel is formulated as follows

$$C = \max_{p(x)} \int_0^\infty I\left(X; Y|h\right) f_h(h) dh, \tag{11}$$

where $I\left(X; Y|h\right)$ is defined as the conditional mutual information between the input X and the output Y given an oceanic turbulence state h. Notice that the capacity is defined as the maximum

Optics EXPRESS

average mutual information which is found over all possible input distributions $p(x)$ that satisfy the average optical power constraint of P_t. As stated in Section 1, we compute, for the first time, the channel capacity of UOWC systems for non-uniform OOK modulation, as previously adopted in the context of terrestrial FSO communication systems through atmospheric turbulence with no ISI [38–40]. In this way, the non-negativity constraint is also satisfied due to the fact that a unidimensional signal space is considered where one constellation point is 0 and the other one is the Euclidean distance $d_E = (1/p)P_t\sqrt{T_b}$. This approach implies that $\mathbb{E}[X^2] \leq pd_E^2$. Thus, knowing that the capacity is obtained when the input X is a zero-mean Gaussian random variable, i.e., $X \sim N\left(0, \sigma_{X_{el}}^2\right)$ [30,37], the conditional mutual information is upper bounded by

$$\begin{aligned} I(X;Y|h) \leq I^G(X;Y|h) &= \frac{1}{2}\log_2\left(1+\frac{\sigma_{X_{el}}^2}{N_0/2}\right) = \frac{1}{2}\log_2\left(1+\frac{\left(\frac{1}{p}-1\right)P_t^2T_bh^2}{N_0/2}\right) \\ &= \frac{1}{2}\log_2\left(1+\left(\frac{1}{p}-1\right)\gamma^2h^2\right), \end{aligned} \tag{12}$$

where $\sigma_{X_{el}}^2 = \mathbb{E}[X_{el}^2] - \mathbb{E}[X_{el}]^2 = ((1/p)-1)P_t^2T_bh^2$ is the variance of the undersea optical intensity detected in electrical domain as a direct consequence of using a non-uniform input distribution [40], $\mathbb{E}[X_{el}^2] = pd_E^2h^2$, $\mathbb{E}[X_{el}] = pd_Eh$, and $\gamma = P_t\sqrt{T_b}/\sigma_n$ is defined as the optical signal-to-noise-ratio (SNR) in the absence of oceanic turbulence. We turn now to the case studio of UOWC channels with ISI memory, i.e, the memory is due to previous inputs alone. In this sense, taking into account that the input symbols are subject to an average optical power constraint of P_t, or equivalently subject to an average electrical power constraint of $pd_E^2h^2$, the conditional mutual information of the UOWC channel with ISI in bits per channel use can be upper bounded as in [22–24], yielding

$$I(X;Y|h) \leq I^G(X;Y|h) = \frac{1}{\pi}\int_0^\pi \frac{1}{2}\log_2\left(1+\left(\frac{1}{p}-1\right)\gamma^2h^2|C(\omega)|^2\right)d\omega, \tag{13}$$

where $|C(\omega)|$ is determined by Eq. (5). Note that, for the capacity to be finite, the sufficient condition is that the energy of the unit-sample response of the filter c_k has to be finite [23]. Then, an upper bound on the average MI of the UOWC system in the presence of ISI and oceanic turbulence can be derived by averaging the above integral over the PDF of h in Eq. (7) as follows

$$I^G(X;Y) \simeq \int_0^\infty \left[\frac{1}{\pi}\int_0^\pi \frac{1}{2}\log_2\left(1+\left(\frac{1}{p}-1\right)\gamma^2h^2|\hat{C}(\omega)|^2\right)d\omega\right]f_h(h)dh \leq H_B(p), \tag{14}$$

where $H_B(p) = -p\log_2 p - (1-p)\log_2(1-p)$ is the binary entropy function that is considered as the maximum mutual information. Unfortunately, the above integral cannot be expressed in closed-form. In order to provide a closed-form expression to compute $I^G(X;Y)$ with high precision, we obtain an approximation for such an upper bound when the parameter b tends to zero, i.e., when $|\hat{C}(\omega)|^2 \simeq a^2\ \forall\ |\omega| \leq \pi$, given by

$$I^G(X;Y) \simeq \frac{1}{\ln 4}\int_0^\infty \ln\left(1+\left(\frac{1}{p}-1\right)a^2\gamma^2h^2\right)f_h(h)dh \leq H_B(p). \tag{15}$$

In order to solve the above integral, we can use the fact that both $\exp(-z)$ and $\ln(1+z)$ can be expressed in terms of the Meijer's G-function $G_{p,q}^{m,n}[\cdot]$ [41, Eq. (7.811)] as $\exp(-z) = G_{0,1}^{1,0}[z|0]$ [42, Eq. (01.03.26.0004.01)] and $\ln(1+z) = G_{2,2}^{1,2}\left[z\middle|_{1,0}^{1,1}\right]$ [42, Eq. (01.04.26.0003.01)], respectively.

Optics EXPRESS

As a result, an approximate closed-form expression for the upper bound on average MI is written in terms of the well-known H-Fox function $H_{p,q}^{m,n}[\cdot]$ [43, Eq. (1.1)] as follows

$$I^G(X;Y) \simeq \frac{1}{\ln 4} H_{3,2}^{1,3}\left[\left(\frac{1}{p}-1\right)a^2\beta_2^2\gamma^2 \,\middle|\, \begin{matrix}(1,1),(1,1),(0,2/\beta_2)\\(1,1),(0,1)\end{matrix}\right] \leq H_B(p). \tag{16}$$

The above approximation can be interpreted as an upper bound on average MI of an ISI-less UOWC channel where the parameter a acts as a power degradation factor due to the ISI. The accuracy of such an expression will be checked in the next Section where a numerical integration for Eq. (14) will be also discussed when no approximations are used. Finally, an upper bound on channel capacity in bits per channel use is found numerically by maximizing the above closed-form expression over the input distribution p as follows

$$C^G = \max_p I^G(X;Y). \tag{17}$$

For comparison purposes, the classical AWGN channel capacity in the absence of ISI and oceanic turbulence is obtained as

$$C_{AWGN}^G = \max_p I_{AWGN}^G(X;Y) = \max_p \left\{\frac{1}{2}\log_2\left(1+\left(\frac{1}{p}-1\right)\gamma^2\right)\right\}. \tag{18}$$

3.2. Channel capacity with a binary input constraint

Now, we compute numerically the mutual information of the UOWC channel under study using non-uniform OOK modulation when a binary input constraint is imposed. Thus, the input-output relation of the UOWC system with ISI and oceanic turbulence was defined in Eq. (3) as

$$Y_k = Ah\sum_{n=0}^{M} c_n X_{k-n} + Z_k, \tag{19}$$

where $A = (1/p)\gamma$, $X_k \in \{0,1\}$ are i.i.d. random variables following a Bernoulli distribution with parameter p, and $Z_k \sim N(0,1)$ due to the fact that the above statistical channel model is normalized by replacing Y_k with Y_k/σ_n. In this way, the conditional mutual information for the UOWC channel with ISI subject to a binary input constraint is defined, as in [44, Section 4.6], as

$$\begin{aligned} I^b(X;Y|h) &= \sum_{i=0}^{1} P(x_i) \\ &\times \int_{-\infty}^{\infty} f_Y\left(y|x_i,x_{i-1},\ldots,x_{i-M},h\right)\log_2\left(\frac{f_Y\left(y|x_i,x_{i-1},\ldots,x_{i-M},h\right)}{\sum_{j=0}^{1}P(x_j)f_Y\left(y|x_j,x_{j-1},\ldots,x_{j-M},h\right)}\right)dy, \end{aligned} \tag{20}$$

where $P(x_i=1)=p$, $P(x_i=0)=1-p$, and $f_Y\left(y|x_i,x_{i-1},\ldots,x_{i-M},h\right)$ represents the PDF of a channel output given the current channel input, yielding

$$f_Y\left(y|x_i=0,x_{i-1},\ldots,x_{i-M},h\right) = \frac{1}{\sqrt{2\pi}}\sum_{r=1}^{2^M} P(\mathbb{X}_r)\exp\left[-\left(y-Ah\sum_{n=1}^{M}c_n x_{i-n}\right)^2/2\right], \tag{21a}$$

$$f_Y\left(y|x_i=1,x_{i-1},\ldots,x_{i-M},h\right) = \frac{1}{\sqrt{2\pi}}\sum_{r=1}^{2^M} P(\mathbb{X}_r)\exp\left[-\left(y-Ahc_0-Ah\sum_{n=1}^{M}c_n x_{i-n}\right)^2/2\right]. \tag{21b}$$

Note that $f_Y\left(y|x_i,x_{i-1},\ldots,x_{i-M},h\right)$ depends on the probabilities assignment on the ISI sequence $\mathbb{X}_r = \{x_{i-1},\ldots,x_{i-M}\}$ where $P(\mathbb{X}_r)$ is the probability of the sequence $\mathbb{X}_r$. Since M is the length of

Optics EXPRESS

the channel impulse response tail, 2^M is the number of possible ISI sequences to be considered due to the fact that x_{i-n} takes on the values 0 and 1. For instance, if $M = 2$ and $\mathbb{X}_r = \{x_{i-1} = 1, x_{i-2} = 0\}$, then $P(\mathbb{X}_r) = p(1-p)$, and so on. Thus, the average MI, $I^b(X;Y)$, can be obtained by averaging Eq. (20) over the PDF of h in Eq. (7) as follows

$$I^b(X;Y) = \int_0^\infty I^b(X;Y|h) f_h(h) dh. \tag{22}$$

Finally, the capacity in bits per channel use is found numerically by maximizing the above average MI over the input distribution p as follows

$$C^b = \max_p I^b(X;Y). \tag{23}$$

It should be noted that a closed-form expression for C^b is not known. In other words, it is not possible to obtain a solution for $I^b(X;Y)$ and C^b formulas given in Eq. (20) and (23) and, hence, they will be evaluated in the next Section via numerical optimization methods available in standard mathematical software packages, as well as the Gaussian upper bound on channel capacity C^G obtained in Eq. (17). In particular, the above expression is really time-consuming and technically difficult to compute. Furthermore, the complexity of the above expression grows with M as it increases the number of possible ISI sequences. Motivated by this, we provide now useful upper and lower bounds on mutual information subject to a binary input constraint that result in being tighter as the ISI becomes less significant.

Firstly, the upper bound is obtained in terms of the average MI of a memoryless UOWC channel with input X_k and output $Y_k = \sqrt{\rho_{UB}} A X_k + Z_k$, where ρ_{UB} is understood as a power improvement due to the memory caused by the ISI coefficients [24,25]. Thus, the factor ρ_{UB} is derived from the norm of c_k as follows

$$\rho_{UB} = ||c||^2 = \sum_{n=0}^{M} |c_n|^2 = \frac{1}{\pi} \int_0^\pi |C(\omega)|^2 d\omega. \tag{24}$$

Secondly, the lower bound is also obtained in terms of the average MI of a memoryless UOWC channel with input X_k and output $Y_k = \rho_{LB} A X_k + Z_k$. Unlike ρ_{UB}, the factor ρ_{LB} is understood as a power degradation due to the memory caused by the ISI coefficients. Thus, ρ_{LB} is obtained, as in [24,25], as follows

$$\rho_{LB} = \exp\left(\frac{1}{\pi} \int_0^\pi \ln |C(\omega)|^2 d\omega \right). \tag{25}$$

Finally, the average MI, $I^b(X;Y)$, can be upper and lower bounded in terms of the average MI of a memoryless UOWC channel as

$$I^b_{LB}(X;Y) \le I^b(X;Y) \le I^b_{UB}(X;Y). \tag{26}$$

Note that the above bounds are computed from Eqs. (20) and (21) for an ISI-less UOWC channel, i.e., when $M = 0$ and $c_0 = 1$.

4. Numerical results and discussion

sIn this section, the new bounds on channel capacity and mutual information of UOWC systems with ISI over oceanic turbulence channels in bits/channel use are computed and tested by Monte Carlo simulations. In particular, UOWC channels with one, two and three ISI coefficients i.e., ISI memory of degree one, two and three, are analyzed. The major UOWC system parameters are summarized in Table 2 where different link distances are considered for clear ocean and

Optics EXPRESS

Table 2. UOWC system parameters.

Parameter	Symbol	Value
Wavelength	λ	532 nm
Responsivity	R	1 Amps per Watt
LD divergence angle at $1/e$	θ	10 mrad
Photodetector diameter	D	20 cm
Receiver field-of-view	FOV	180°
Link distance (Clear ocean water)	d	$\{30, 40, 50\}$ m
Link distance (Coastal water)	d	$\{15, 25, 35\}$ m

coastal waters as practical scenarios according to previous reported papers [11–13], and available commercial systems such as those provided by Sonardyne for link distances up to 150 m [45]. At the transmitter side, a green LD is used with a transmit divergence angle of $\theta = 10$ mrad while,

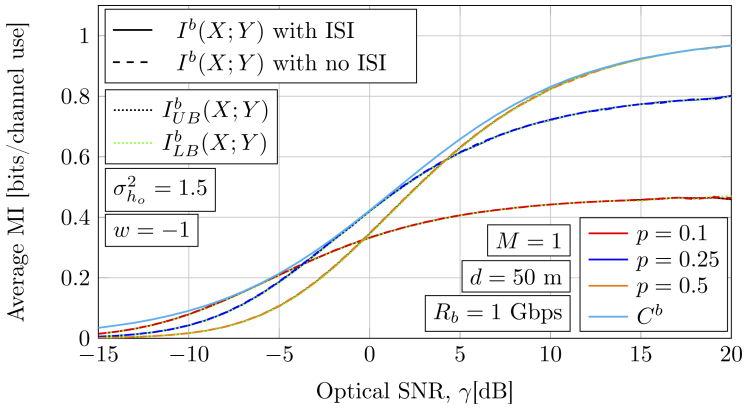

(a) $R_b = 1$ Gbps

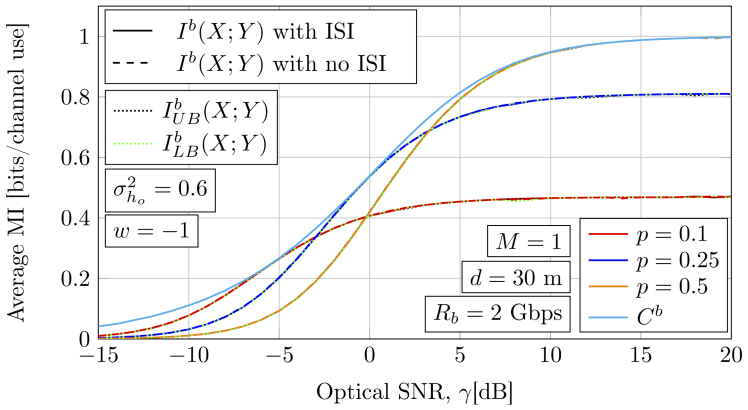

(b) $R_b = 2$ Gbps

Fig. 3. Average MI, $I^b(X;Y)$, and channel capacity, C^b, for clear ocean water when the data rate equals $R_b = 1$ Gbps (a), and equals $R_b = 2$ Gbps (b) in the presence of ISI and salinity-induced oceanic turbulence when. A photodetector diameter of $D = 20$ cm and a FOV of 180° are considered. Both channel capacity and average MI for ISI-less channels are also plotted by using dashed line.

Optics EXPRESS

at the receiver side, a photodetector diameter of $D = 20$ cm and a FOV of 180° are assumed. Regarding oceanic turbulence, the scintillation index expressed in Eq. (9) can be calculated numerically or using the approximate closed-form expression developed in [9, Appendix A], as well as the parameters β_1 and β_2 are calculated from Eq. (8). Scintillation index values of $\sigma_{h_o}^2 = \{0.1, 0.4, 0.6, 0.8, 1, 1.5\}$ are computed for link distances of $d = \{15, 25, 30, 35, 40, 50\}$ m, respectively, which model different salinity-induced oceanic turbulent conditions when $w = -1$, $\epsilon = 10^{-5}\ m^2/s^3$, and $\chi_T = 10^{-7}\ K^2/s$ [34,35]. Without loss of generality, all figures plot channel capacity and mutual information for a normalized path loss of $L = 1$. Nonetheless, path loss values of 29.24 dB, 37.91 dB and 46.10 dB are computed in clear ocean water for link distances of 30 m, 40 m and 50 m, respectively, as well as for the setup outlined in Table 2. Analogously, path loss values of 28.78 dB, 47.92 dB and 64.91 dB are also computed in coastal water for link distances of 15 m, 25 m and 35 m, respectively. These path loss values would induce a right shift in decibels of the current channel capacity and mutual information curves.

In Figs. 3 and 4, the average MI, $I^b(X;Y)$, obtained in Eq. (22) is plotted as a function of the optical SNR γ[dB] when different non-uniform input distributions of $p = \{0.1, 0.25, 0.5\}$ and

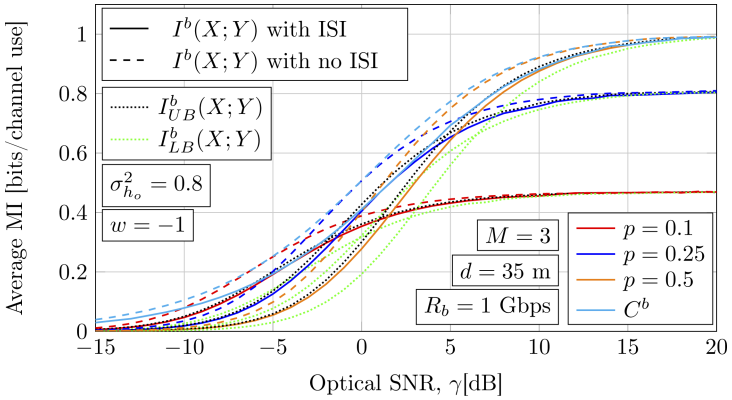

(a) $R_b = 1$ Gbps

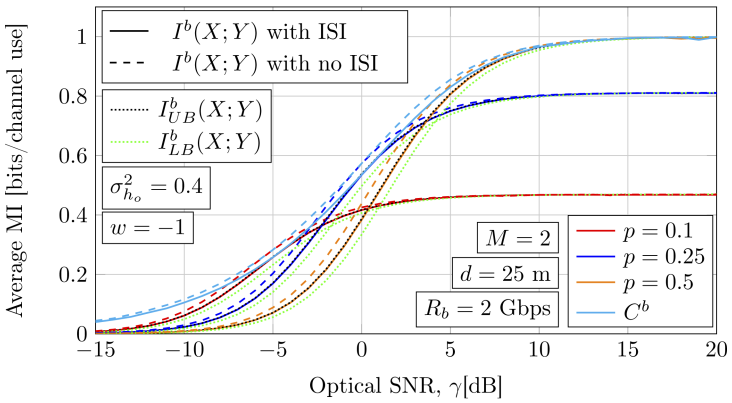

(b) $R_b = 2$ Gbps

Fig. 4. Average MI, $I^b(X;Y)$, and channel capacity, C^b, for coastal water when the data rate equals $R_b = 1$ Gbps (a), and equals $R_b = 2$ Gbps (b) in the presence of ISI and salinity-induced oceanic turbulence. A photodetector diameter of $D = 20$ cm and a FOV of 180° are considered. Both channel capacity and average MI for ISI-less channels are also plotted by using dashed line.

Optics EXPRESS

different symbol rate of $R_b = \{1, 2\}$ Gbps are considered. Additionally, the upper and lower bounds on average MI, i.e., $I^b_{UB}(X;Y)$ and $I^b_{LB}(X;Y)$, are depicted, as well as the channel capacity, C^b, obtained in Eq. (23). Note that all $I^b_{UB}(X;Y)$ results are plotted with a black dotted line, whereas all $I^b_{LB}(X;Y)$ results are plotted with a green dotted line. For comparison purposes, both the average channel capacity and the average MI for ISI-less UOWC channels are also included by using a dashed line. On the one hand, it is verified that the effect of salinity-induced oceanic turbulence cannot be ignored when analyzing both channel capacity and mutual information of UOWC systems, particularly in open waters, as previously concluded using other performance metrics such as BER and outage probability [14–19]. On the other hand, as can be seen in Fig. 3, all results are overlapped due to the fact that scattering is not significant in clear ocean water. In such a case, the impulse response tail equals 1, i.e., $M = 1$. According to these results, the inequality represented in Eq. (26) becomes an equality, concluding that the impact of ISI can be neglected in this kind of water at moderate link distances. On the contrary, in Fig. 4, the ISI degrades both average channel capacity and average MI by inducing an optical SNR penalty of a few decibels with respect to the case of an ISI-less channel. This optical SNR penalty depends mainly on scattering, link distance and data rate. In coastal water, it is observed that the upper bound, $I^b_{UB}(X;Y)$, results in being much tighter and useful than the lower one, $I^b_{LB}(X;Y)$, relaxing

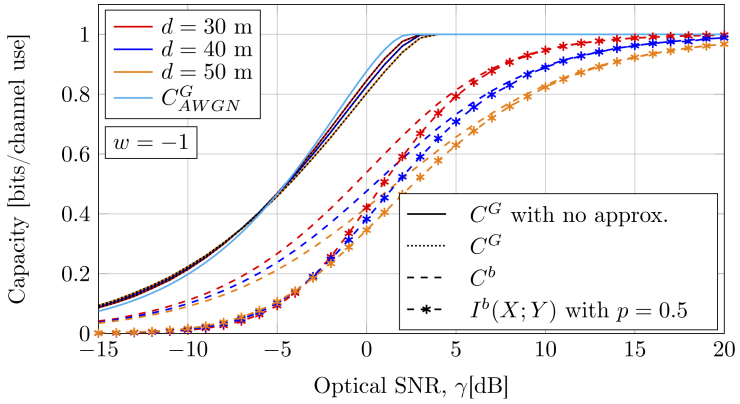

(a) Clear ocean water

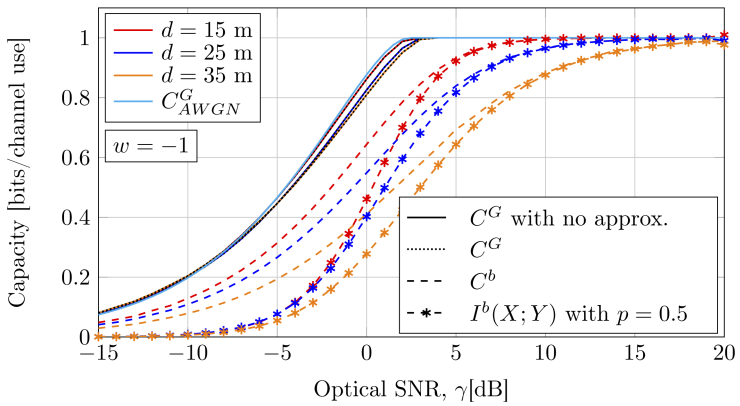

(b) Coastal water

Fig. 5. Channel capacity for (a) clear ocean, and (b) coastal waters in the presence of ISI and salinity-induced oceanic turbulence when a photodetector diameter of $D = 20$ cm, a FOV of 180°, as well as a data rate of $R_b = 1$ Gbps are considered.

Optics EXPRESS

the computational load as required to compute Eq. (22). As expected, this upper bound is even tighter as the ISI becomes less significant. Interestingly, we have quantified what it was already anticipated qualitatively in Section 2 from the DFT of c_k with regard to the impact of ISI on channel capacity. It is observed that the ISI severely degrades channel capacity when the level of impurities of water increases, as noted in Section 2.

In Fig. 5, the Gaussian upper bound on channel capacity, C^G, obtained in Eq. (17), as well as the channel capacity, C^b, obtained in Eq. (23) subject to a binary constraint are plotted as a function of the optical SNR γ[dB]. Both channel capacity derivations are computed by using numerical optimization methods that are available in standard mathematical software packages. Firstly, it is corroborated that the Gaussian upper bound, C^G, which is obtained via maximization of the approximate average mutual information as derived in terms of the H-Fox function in Eq. (17) achieves a high accuracy for the whole range of optical SNR considered in both figures. Such capacity results match very well with the Gaussian upper bound, C^G, obtained via Monte Carlo simulations from Eq. (14) when no approximations (labeled C^G with no approx.) are used in all practical UOWC scenarios analyzed. For comparison purposes, these figures also plot

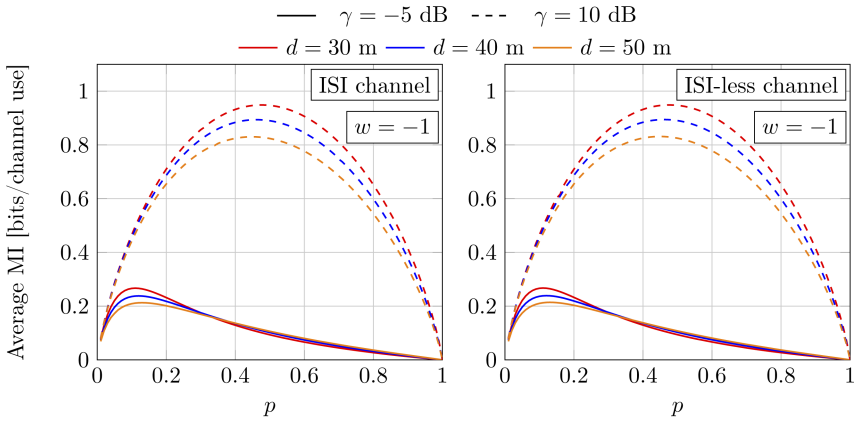

(a) Clear ocean water

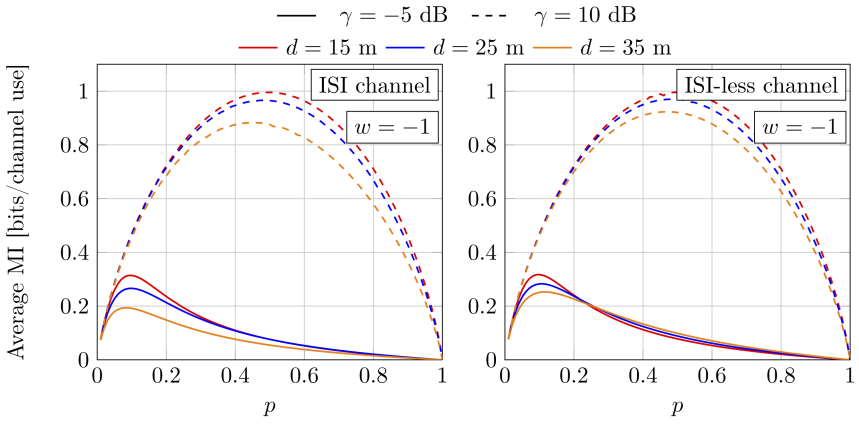

(b) Coastal water

Fig. 6. Average MI, $I^b(X;Y)$, as a function of the non-uniform input distribution p for (a) clear ocean, and (b) coastal waters in the presence of ISI and salinity-induced oceanic turbulence when a photodetector diameter of D = 20 cm, a FOV of 180°, as well as a data rate of R_b = 1 Gbps are considered.

Optics EXPRESS

the average MI for uniform distribution with $p = 0.5$ when the same average optical power as the non-uniform distribution is assumed. Additionally, these figures plot the classical AWGN channel capacity, C^{G}_{AWGN}, obtained in Eq. (18) as a reference. As expected, the ISI does not make channel capacity increase, quite the contrary. The combined effect of scattering-induced ISI and oceanic turbulence impacts drastically on channel capacity of the UOWC system. Moreover, all the average mutual information and capacity results tend asymptotically to the binary entropy function $H_B(p)$ as the optical SNR increases where values of $H_B(p) = \{1, 0.811, 0.468\}$ are computed for input distributions of $p = \{0.5, 0.25, 0.1\}$, respectively.

Finally, it is concluded that the capacity-achieving distribution, which is obtained through numerical optimization, is discrete and can be expressed analytically as $f_X(x) = (1-p)\delta(x) + p\delta(x - d_E)$ with $\delta(\cdot)$ being the Dirac delta function, and p being obtained numerically for each optical SNR value. It is highlighted that this non-uniform input distribution notably improves the channel capacity of the UOWC system in the presence of ISI and oceanic turbulence particularly at low optical SNR, as also corroborated in the context of terrestrial FSO systems with no ISI [39,40]. In fact, this key feature can be also observed from another interesting viewpoint as illustrated in Fig. 6. In such a figure, the average MI, $I^b(X;Y)$, is plotted as a function of the non-uniform input distribution p when different optical SNR values of $\gamma = \{-5, 10\}$ dB are considered in order to corroborate that the optimum values of p fundamentally change with each value of the optical SNR and do not depend on the severity of the ISI. Similar conclusions can be drawn from this figure to those previously obtained when comparing clear ocean and coastal waters.

5. Conclusion

In this paper, novel insights into the combined impact of scattering-induced ISI and salinity-induced oceanic turbulence on channel capacity and mutual information have been provided when different constraints were imposed on the channel input.

On the one hand, a new upper bound on channel capacity subject to non-negative and average optical power constraints has been found by using the DFT of the equivalent discrete-time impulse response of the UOWC system when the channel inputs are Gaussian random variables with fixed average optical power. In the light of this research, it was verified that channel capacity is clearly affected not only by salinity-induced oceanic turbulence, but also by scattering-induced ISI. Both degrading factors cannot be neglected from an information-theoretical viewpoint. On the other hand, it is concluded that, in clear ocean water, channel capacity subject to a binary input constraint can be well approximated by the channel capacity with no ISI where the derived upper and lower bounds converge on the same bound under negligible scattering conditions. However, in coastal water, different conclusions are obtained. The effect of scattering is dominating the capacity, and the originated ISI incurs a significant optical SNR penalty in terms of rate when comparing with an ISI-less channel. Despite the fact that the lower bound on channel capacity is not the tightest possible in coastal water, the upper one results in being remarkably tight. Furthermore, it is able to achieve a substantial computational reduction in general terms since channel capacity is computed from the channel capacity of the UOWC system with no ISI by adding a power coefficient due to the memory introduced by the ISI. Finally, due to the similarities between undersea and terrestrial free-space communications, it is thought that non-uniform signalling algorithms developed for terrestrial FSO systems to generate linear binary codes might be implemented in the context of UOWC systems with ISI.

In the near future, the use of passband modulation schemes and multiple inputs and/or multiple outputs structures should be explored to try to mitigate the impact of scattering-induced ISI and oceanic turbulence on channel capacity and practical information rates while narrow-beam LD are used to enable fast, long-distance undersea communications.

Optics EXPRESS

A. Results of equivalent discrete-time impulse response

In this appendix, we show some results of the equivalent discrete-time response of different practical UOWC scenarios for clean ocean (Table 3) and coastal (Table 4) waters. Moreover, the value of each length of the channel impulse response tail, M, is also listed in both Tables. The parameters a and b from which the DFT is modeled for each scenario are also provided along with the corresponding value of the coefficient of determination R^2. Note that $\mathbb{C}(t)$ is evaluated

Table 3. Equivalent discrete-time impulse response for clear ocean water.

Distance	R_b = 0.5 Gbps	R_b = 1 Gbps	R_b = 2 Gbps
d = 30 m	$c_0 = 0.9987; c_1 = 0.001324$ $(a, b) = (0.9987, 0.001324)$ $M = 1; R^2 = 0.999$	$c_0 = 0.99754; c_1 = 0.0026$ $(a, b) = (0.99754, 0.0026)$ $M = 1; R^2 = 0.997$	$c_0 = 0.9952; c_1 = 0.0048$ $(a, b) = (0.9952, 0.0048)$ $M = 1; R^2 = 0.991$
d = 40 m	$c_0 = 0.997; c_1 = 0.003$ $(a, b) = (0.997, 0.003)$ $M = 1; R^2 = 0.998$	$c_0 = 0.9944; c_1 = 0.0055$ $(a, b) = (0.9945, 0.0055)$ $M = 1; R^2 = 0.993$	$c_0 = 0.99; c_1 = 0.01$ $(a, b) = (0.99, 0.01)$ $M = 1; R^2 = 0.983$
d = 50 m	$c_0 = 0.9947; c_1 = 0.0053$ $(a, b) = (0.9947, 0.0053)$ $M = 1; R^2 = 0.995$	$c_0 = 0.9903; c_1 = 0.0097$ $(a, b) = (0.9903, 0.0097)$ $M = 1; R^2 = 0.986$	$c_0 = 0.9831; c_1 = 0.0169$ $(a, b) = (0.983, 0.014)$ $M = 1; R^2 = 0.971$

via Monte Carlo simulation based on photon tracing which makes use of the Henyey-Greenstein phase function as the scattering angular distribution in seawater, as described in greater detail in [21]. All these results have been obtained by considering the system parameters summarized in Tables 1 and 2. The results outlined in Table 3 for clear ocean water demonstrate that, under these scattering conditions, the equivalent discrete-time channel can be modeled as a linear filter with only one coefficient, i.e., $M = 1$, achieving a value of R^2 above 0.97 when different data rate values of $R_b = \{0.5, 1, 2\}$ Gbps are considered. In other words, the impact of ISI on channel capacity under clear ocean water conditions can be neglected when the data rate is below a few Gbps. However, under coastal water conditions, the situation is quite different since the effect of

Table 4. Equivalent discrete-time impulse response for coastal water.

Distance	R_b = 0.5 Gbps	R_b = 1 Gbps	R_b = 2 Gbps
d = 15 m	$c_0 = 0.9934; c_1 = 0.0066$ $(a, b) = (0.9934, 0.0066)$ $M = 1; R^2 = 0.997$	$c_0 = 0.9879; c_1 = 0.0121$ $(a, b) = (0.9879, 0.0121)$ $M = 1; R^2 = 0.987$	$c_0 = 0.9794; c_1 = 0.0206$ $(a, b) = (0.9794, 0.0206)$ $M = 1; R^2 = 0.957$
d = 25 m	$c_0 = 0.9504; c_1 = 0.0496$ $(a, b) = (0.9504, 0.0496)$ $M = 1; R^2 = 0.988$	$c_0 = 0.9194; c_1 = 0.0806$ $(a, b) = (0.9194, 0.0806)$ $M = 1; R^2 = 0.953$	$c_0 = 0.8807; c_1 = 0.0775$ $c_2 = 0.0418$ $(a, b) = (0.8807, 0.1193)$ $M = 2; R^2 = 0.866$
d = 35 m	$c_0 = 0.8095; c_1 = 0.1435$ $c_2 = 0.045$ $(a, b) = (0.8095, 0.1905)$ $M = 2; R^2 = 0.889$	$c_0 = 0.7101; c_1 = 0.1788$ $c_2 = 0.0881; c_3 = 0.0232$ $(a, b) = (0.7101, 0.2899)$ $M = 3; R^2 = 0.88$	$c_0 = 0.6235; c_1 = 0.1732$ $c_2 = 0.0722; c_3 = 0.04$ $c_4 = 0.032; c_5 = 0.0241$ $c_6 = 0.0161; c_7 = 0.01; c_8 = 0.0085$ $(a, b) = (0.6235, 0.3764)$ $M = 8; R^2 = 0.878$

scattering becomes significant even when the data rate is not too high, i.e., as R_b approaches infinity, the value of M also approaches infinity, as deduced from Table 4. In this case, the

Optics EXPRESS

equivalent discrete-time channel can be modeled as a linear filter with more than one coefficient, achieving a value of R^2 above 0.87 for data rate values of $R_b = \{0.5, 1, 2\}$ Gbps.

Funding. Programa Operativo I+D+i FEDER Andalucía 2014-2020 (P18-RTJ-3343); Spanish MICINN (PID2019-107792GB-I00).

Disclosures. The authors declare no conflicts of interest.

Data availability. Data underlying the results presented in this paper are not publicly available at this time but may be obtained from the authors upon reasonable request.

References

1. Z. Zeng, S. Fu, H. Zhang, Y. Dong, and J. Cheng, "A survey of underwater optical wireless communications," IEEE Commun. Surv. Tutorials **19**(1), 204–238 (2017).
2. X. Sun, C. H. Kang, M. Kong, O. Alkhazragi, Y. Guo, M. Ouhssain, Y. Weng, B. H. Jones, T. K. Ng, and B. S. Ooi, "A review on practical considerations and solutions in underwater wireless optical communication," J. Lightwave Technol. **38**(2), 421–431 (2020).
3. C. D. Mobley, *Light and water: radiative transfer in natural waters* (Academic, 1994).
4. M. V. Jamali, A. Chizari, and J. A. Salehi, "Performance analysis of multi-hop underwater wireless optical communication systems," IEEE Photonics Technol. Lett. **29**(5), 462–465 (2017).
5. M. V. Jamali, P. Nabavi, and J. A. Salehi, "MIMO underwater visible light communications: Comprehensive channel study, performance analysis, and multiple-symbol detection," IEEE Trans. Veh. Technol. **67**(9), 8223–8237 (2018).
6. M. V. Jamali, A. Mirani, A. Parsay, B. Abolhassani, P. Nabavi, A. Chizari, P. Khorramshahi, S. Abdollahramezani, and J. A. Salehi, "Statistical studies of fading in underwater wireless optical channels in the presence of air bubble, temperature, and salinity random variations," IEEE Trans. Commun. **66**(10), 1 (2018).
7. A. Jurado-Navas, N. G. Serrato, J. Garrido-Balsells, and M. Castillo-Vázquez, "Error probability analysis of OOK and variable weight MPPM coding schemes for underwater optical communication systems affected by salinity turbulence," OSA Continuum **1**(4), 1131–1143 (2018).
8. E. Zedini, H. M. Oubei, A. Kammoun, M. Hamdi, B. S. Ooi, and M.-S. Alouini, "Unified statistical channel model for turbulence-induced fading in underwater wireless optical communication systems," IEEE Trans. Commun. **67**(4), 2893–2907 (2019).
9. R. Boluda-Ruiz, A. García-Zambrana, B. Castillo-Vázquez, and S. Hranilovic, "Impact of angular pointing error on BER performance of underwater optical wireless links," Opt. Express **28**(23), 34606–34622 (2020).
10. A. S. Ghazy, S. Hranilovic, and M.-A. Khalighi, "Angular MIMO for Underwater Wireless Optical Communications: Link Modelling and Tracking," IEEE J. Oceanic Engineering In press. hal-03147572.
11. W. Lyu, M. Zhao, X. Chen, X. Yang, Y. Qiu, Z. Tong, and J. Xu, "Experimental demonstration of an underwater wireless optical communication employing spread spectrum technology," Opt. Express **28**(7), 10027–10038 (2020).
12. J. Du, Y. Wang, C. Fei, R. Chen, G. Zhang, X. Hong, and S. He, "Experimental demonstration of 50-m/5-Gbps underwater optical wireless communication with low-complexity chaotic encryption," Opt. Express **29**(2), 783–796 (2021).
13. X. Liu, S. Yi, X. Zhou, Z. Fang, Z.-J. Qiu, L. Hu, C. Cong, L. Zheng, R. Liu, and P. Tian, "34.5 m underwater optical wireless communication with 2.70 Gbps data rate based on a green laser diode with NRZ-OOK modulation," Opt. Express **25**(22), 27937–27947 (2017).
14. H. Zhang, J. Cheng, Z. Wang, and Y. Dong, "On the capacity of buoy-based MIMO systems for underwater optical wireless links with turbulence," in *2018 IEEE International Conference on Communications (ICC)*, (2018), pp. 1–6.
15. Y. Li, Y. Zhang, and Y. Zhu, "Capacity of underwater wireless optical links with pointing errors," Opt. Commun. **446**, 16–22 (2019).
16. M. C. Gökçe, "Average capacity analysis of underwater optical wireless communication links over anisotropic strong oceanic turbulence channels," J. Opt. Soc. Am. A **36**(12), 2040–2047 (2019).
17. G. Xu and J. Lai, "Average capacity analysis of the underwater optical plane wave over anisotropic moderate-to-strong oceanic turbulence channels with the Málaga fading model," Opt. Express **28**(16), 24056–24068 (2020).
18. G. Xu, Z. Song, and Q. Zhang, "Outage probability and channel capacity of an optical spherical wave propagating through anisotropic weak-to-strong oceanic turbulence with Málaga distribution," J. Opt. Soc. Am. A **37**(10), 1622–1629 (2020).
19. M. C. Gökçe, "Effect of adaptive optics on average channel capacity of underwater optical wireless communication system," in *2020 IEEE Innovations in Intelligent Systems and Applications Conference (ASYU)*, (2020), pp. 1–5.
20. C. Gabriel, M.-A. Khalighi, S. Bourennane, P. Léon, and V. Rigaud, "Monte-Carlo-based channel characterization for underwater optical communication systems," J. Opt. Commun. Netw. **5**(1), 1–12 (2013).
21. R. Boluda-Ruiz, P. Rico-Pinazo, B. Castillo-Vazquez, A. Garcia-Zambrana, and K. Qaraqe, "Impulse response modeling of underwater optical scattering channels for wireless communication," IEEE Photonics J. **12**(4), 1–14 (2020).
22. L. Brandenburg and A. Wyner, "Capacity of the Gaussian channel with memory: The multivariate Case," Bell Syst. Tech. J. **53**(5), 745–778 (1974).

Optics EXPRESS

23. W. Hirt and J. L. Massey, "Capacity of the discrete-time Gaussian channel with intersymbol Interference," IEEE Trans. Inf. Theory **34**(3), 38 (1988).
24. S. Shamai, L. H. Ozarow, and A. D. Wyner, "Information rates for a discrete-time Gaussian channel with intersymbol interference and stationary inputs," IEEE Trans. Inf. Theory **37**(6), 1527–1539 (1991).
25. S. Shamai and R. Laroia, "The intersymbol interference channel: Lower bounds on capacity and channel precoding loss," IEEE Trans. Inf. Theory **42**(5), 1388–1404 (1996).
26. Y. Carmon and S. S. Shitz, "Lower bounds and approximations for the information rate of the ISI channel," IEEE Trans. Inf. Theory **61**(10), 5417–5431 (2015).
27. J. M. Kahn and J. R. Barry, "Wireless infrared communications," Proc. IEEE **85**(2), 265–298 (1997).
28. M. A. Khalighi and M. Uysal, "Survey on free space optical communication: A communication theory perspective," IEEE Commun. Surv. Tutorials **16**(4), 2231–2258 (2014).
29. A. Chaaban and S. Hranilovic, "Capacity of optical wireless communication channels," Phil. Trans. R. Soc. A **378**(2169), 20190184 (2020).
30. J. G. Proakis, *Digital Communications* (McGraw-Hill International Editions, 1995).
31. H. M. Oubei, E. Zedini, R. T. ElAfandy, A. Kammoun, T. K. Ng, M.-S. Alouini, and B. S. Ooi, "Efficient Weibull channel model for salinity induced turbulent underwater wireless optical communications," in *IEEE Opto-Electronics and Communications Conference (OECC) and Photonics Global Conference (PGC)*, (2017), pp. 1–2.
32. A. Jurado-Navas, J. M. Garrido-Balsells, M. Castillo-Vazquez, A. García-Zambrana, and A. Puerta-Notario, "Converging underwater and FSO ground communication links," in *2019 Optical Fiber Communications Conference and Exhibition (OFC)*, (2019), pp. 1–3.
33. L. C. Andrews and R. L. Phillips, *Laser beam propagation through random media*, vol. 1 (SPIE, Bellingham, WA, 2005).
34. V. Nikishov and V. Nikishov, "Spectrum of turbulent fluctuations of the sea-water refraction index," Int. J. Fluid Mech. Res. **27**(1), 82–98 (2000).
35. O. Korotkova, N. Farwell, and E. Shchepakina, "Light scintillation in oceanic turbulence," Waves in Random and Complex Media **22**(2), 260–266 (2012).
36. S. A. Thorpe, *The turbulent ocean* (Cambridge University, 2005).
37. T. M. Cover and J. A. Thomas, *Elements of Information Theory* (Wiley & Sons, New York, 2006), 2nd ed.
38. S. Hranilovic and F. R. Kschischang, "Capacity bounds forpower- and band-limited optical intensity channels corrupted by Gaussian noise," IEEE Trans. Inf. Theory **50**(5), 784–795 (2004).
39. A. Farid and S. Hranilovic, "Channel capacity and non-uniform signalling for free-space optical intensity channels," IEEE J. Sel. Areas Commun. **27**(9), 1553–1563 (2009).
40. A. García-Zambrana, B. Castillo-Vázquez, and C. Castillo-Vázquez, "Average capacity of FSO links with transmit laser selection using non-uniform OOK signaling over exponential atmospheric turbulence channels," Opt. Express **18**(19), 20445–20454 (2010).
41. I. S. Gradshteyn and I. M. Ryzhik, *Table of integrals, series and products* (Academic Inc., 2007), 7th ed.
42. Wolfram Research, Inc., "The Wolfram functions site,".
43. A. A. Kilbas, *H-transforms: Theory and Applications* (CRC, 2004).
44. R. G. Gallager, *Information Theory and Reliable Communications* (Wiley, New York, 1968).
45. "The Sonardyne site: Bluecomm underwater optical communications. Sonardyne International ltd.," http://www.sonardyne.com/.